Mechanics of Biomimetic Liposomes Encapsulating an Actin Shell

Karine Guevorkian, John Manzi, Léa-Lætitia Pontani, Françoise Brochard-Wyart, C. Sykes

Article

Mechanics of Biomimetic Liposomes Encapsulating an Actin Shell

Karine Guevorkian,[1,2,3] John Manzi,[1,2] Léa-Lætitia Pontani,[4] Françoise Brochard-Wyart,[1,2] and Cécile Sykes[1,2,*]
[1]Laboratoire Physico Chimie Curie, Institut Curie, PSL Research University, CNRS UMR168, Paris, France; [2]Sorbonne Universités, UPMC Univ Paris 06, Paris, France; [3]Institut de Génétique et de Biologie Moléculaire et Cellulaire, Université de Strasbourg, Centre National de la Recherche Scientifique, UMR 7104, Institut National de la Santé et de la Recherche Médicale, U964, Illkirch, France; and [4]Institut des Nanosciences de Paris, Université Paris VI, Centre National de la Recherche Scientifique, UMR 7588, Paris, France

ABSTRACT   Cell-shape changes are insured by a thin, dynamic, cortical layer of cytoskeleton underneath the plasma membrane. How this thin cortical structure impacts the mechanical properties of the whole cell is not fully understood. Here, we study the mechanics of liposomes or giant unilamellar vesicles, when a biomimetic actin cortex is grown at the inner layer of the lipid membrane via actin-nucleation-promoting factors. Using a hydrodynamic tube-pulling technique, we show that tube dynamics is clearly affected by the presence of an actin shell anchored to the lipid bilayer. The same force pulls much shorter tubes in the presence of the actin shell compared to bare membranes. However, in both cases, we observe that the dynamics of tube extrusion has two distinct features characteristic of viscoelastic materials: rapid elastic elongation, followed by a slower elongation phase at a constant rate. We interpret the initial elastic regime by an increase of membrane tension due to the loss of lipids into the tube. Tube length is considerably shorter for cortex liposomes at comparable pulling forces, resulting in a higher spring constant. The presence of the actin shell seems to restrict lipid mobility, as is observed in the corral effect in cells. The viscous regime for bare liposomes corresponds to a leakout of the internal liquid at constant membrane tension. The presence of the actin shell leads to a larger friction coefficient. As the tube is pulled from a patchy surface, membrane tension increases locally, leading to a Marangoni flow of lipids. As a conclusion, the presence of an actin shell is revealed by its action that alters membrane mechanics.

INTRODUCTION

The cell cortex is a thin shell of actin that lies underneath the plasma membrane. It is part of the cytoskeleton that controls cell shape. In mammalian cells, this cortex is ~1 μm thick and is attached to the plasma membrane through specific protein links, but also through active proteins that polymerize actin locally (1). The cortex is a substrate for myosin attachment and tension buildup. The role of the cortex is to insure the mechanics of the cellular interface and adapt it to cell fate. For example, just before cell division, cells are able to round up through cortex rearrangements. Given the cell complexity, it is difficult to decipher the role of the different ingredients involved in insuring cell mechanics. Therefore, for the past two decades, simplified biomimetic systems of liposomes (or giant unilamellar vesicles) encapsulated with biological material that mimic cell content have been developed (2,3). In certain experimental conditions in which the membrane tensions are of the order of 10^{-3} N/m, the elastic contribution of the membrane is found to be dominant, masking the role of the cortex on membrane mechanics (4,5). Therefore, the specific contribution of the actin cytoskeleton on the global mechanics of plasma membrane needs to be unveiled in conditions other than pure elasticity measurements.

Spreading dynamics of cell-sized liposomes (4) or tube-pulling dynamics (6) have revealed that the viscous contribution differs in the presence or absence of an actin shell grown from the inner leaflet of the membrane.

Here, we use hydrodynamic tube extrusion (7) to study the viscoelastic mechanics of a liposome, inside which an actin cortex has been produced on the model of the cell: an activator of actin polymerization is linked to the inner leaflet of the liposome, in which the actin machinery is incorporated. We show that the mechanics of such liposomes drastically depend on the presence of the actin shell. We explain that the actin cortex controls the mechanics of the entire cell-sized liposome through changing the mechanical properties of the membrane, both in the elastic and in the viscous regime. Our study confirms the subtle role of the actin cortex in controlling cell mechanics.

MATERIALS AND METHODS

Liposome preparation

Liposomes were prepared using an inverted emulsion technique described by Pontani et al. (3). The lipids EPC, Cholesterol, DOGS-NTA-Ni, and DSPE-PEG(2000)-Biotin (Avanti Polar Lipids, Alabaster, AL) were dissolved in mineral oil (Sigma-Aldrich, St. Louis, MO) at a molar ratio EPC/Cholesterol/DOGS-NTA-Ni/Biotin of 52:37:10:1 at a total concentration of 0.5 mg/mL. The mix was sonicated for 2 h at 50°C and stored up to one week at 4°C. Bulk actin liposomes contained 3 μM actin, in internal buffer ("I-Buffer"). Cortex liposomes contained 3 μM actin, 7.8 μM VVCA-His, 0.45 μM Arp2/3, and 10 μM profilin in I-Buffer. The actin

*Correspondence: cecile.sykes@curie.fr

solution contained 10% fluorescently labeled actin from rabbit muscle (bulk, Alexa Fluor 488 conjugate; cortex, Alexa Fluor 568 conjugate) prepared in G-buffer (general actin buffer). Actin and Arp2/3 were purchased from Cytoskeleton (Denver, CO); the fluorescent actin was purchased from Invitrogen (Carlsbad, CA); and the VVCA-His and profilin were homemade, as previously described in Pontani et al. (3) and Carvalho et al. (8), respectively. The I-Buffer contained 10 mM HEPES (pH 7.5), 0.1 mM CaCl$_2$, 50 mM KCl, 2 mM MgCl$_2$, 5 mM ATP, 1 mM DTT (dithiothreitol), 0.5 mM Dabco (diazabicyclo[2,2,2]octane), 100 mg/mL dextran, and 180 mM sucrose to obtain a total osmolarity of 300 mOsm. The external buffer contained 10 mM HEPES (pH 7.5), 2 mM MgCl$_2$, 0.2 mM CaCl$_2$, 2 mM ATP, 1 mM DTT, 0.5 mM Dabco, 300 mM glucose, and 0.2 mg/mL casein to obtain a total osmolarity of 320 mOsm.

Hydrodynamic tube extrusion

The experimental chamber consisted of a single microfluidic channel made out of PDMS (poly-(dimethylsiloxane)), which was attached to a cover glass through plasma activation. One side of the channel was cut open to allow the introduction of the liposomes and the glass microstick. The other end was connected to an aspiration pump (MFCS-VAC-25 mbar; Fluigent, Villejuif, France), equipped with a debit meter. (A similar system has been previously used to study bare liposomes (7).) The size of the channel was 200 μm high, 600 μm wide, and 2 cm long. A coated glass microstick was used to attach the vesicles. Thin-tip microsticks were prepared by pulling borosilicate rods (1 mm; World Precision Instruments, Sarasota, FL) using a laser-based puller (P-2000; Sutter Instrument, Novato, CA). The rods were then forged to 2–3 μm using a microforge (MF-900; Narishige, Tokyo, Japan). To coat the microsticks, they were first cleaned in a plasma cleaner for 30 s, then incubated in 0.1% v/w PolyL-Lysin (Sigma-Aldrich) in PBS (phosphate-buffered saline) for 30 min, rinsed with PBS, and incubated in 1 mg/mL streptavidin (Sigma-Aldrich) in PBS solution for 1 h. The adhesion of the vesicles to the glass microsticks took place through the streptavidin and the biotinylated lipids in the vesicle membrane. Once the vesicle was attached to the rod, it was brought into the channel using a mechanical micromanipulator and raised to the middle of the channel. Using the aspiration pump, a fixed debit, D, ranging between 20 and 1000 nL/min, was applied. The velocity of the Poiseuille flow, U, at the midheight of the channel is related to D through $U = 1.5 \times D/A_c$, where A_c is the cross section of the channel. For the dimensions of our channel, the flow velocities range between 4 and 200 μm/s.

Imaging and analysis

The imaging was performed using a charge-coupled device camera (CoolSNAP; Photometrics, Tucson, AZ) on an inverted microscope (Model No. IX70; Olympus, Tokyo, Japan). We used ×20 (NA = 0.5) and ×40 (NA = 0.6) objectives depending on the magnification required. The image acquisition rate was 0.5 or 1 frame/s controlled by the MetaMorph interface (Molecular Devices, Eugene, OR). The tracking of the liposomes were done using the MetaMorph software. Further analysis was performed using custom-made MATLAB routines (The MathWorks, Natick, MA).

To adjust the stepwise tube extrusion curves with Eq. 3 as explained in the Discussion section, we modified it as follows to leave the time corresponding to $L = 0$ of each step as a free parameter, t_{n0}. Considering that at time t_n (at which we change the force) that $L = L_n$, Eq. 3 becomes

$$L(t - t_{n0}) = L_n + L_{\text{cross}\_n}\left(e^{-(t_n - t_{n0})/\tau_n} - e^{-(t - t_{n0})/\tau_n}\right)$$
$$+ \dot{L}_{v\_n}(t - t_n). \qquad (1)$$

This equation has four fitting parameters: L_{cross_n}, τ_n, t_{n0}, and $\dot{L}_{v\_n}$. We found that this fit is not very stable, sometimes giving erroneous values

for L_{cross_n}. The parameter range for L_{cross_n} was therefore constrained to $L_n < L_{\text{cross}\_n} < L_n + 30$ μm, where the initialization value for L_{cross_n} was obtained by fitting the beginning of the curve (first 10–15 s, corresponding to the elastic regime) with the first part of Eq. 1 ($\dot{L}_{v\_n} = 0$). Once we have this length, we readjust the data with Eq. 1.

RESULTS

Cortex and bulk liposome systems

The actin machinery (the Arp2/3 complex, VVCA-His, profilin and actin; see Materials and Methods) is incorporated inside liposomes using the inverted emulsion technique as described in Pontani et al. (3), Murrell et al. (4), and Pautot et al. (9). Encapsulation is performed at 4°C, then liposomes are transferred into the experimental chamber and left at room temperature (23°C) to allow actin to polymerize into filaments. The way proteins assemble is shown schematically in Fig. 1 A. Actin nucleation is promoted by a fragment of N-WASP, a nucleation-promoting factor, known as VVCA-His, linked to nickel lipids at the membrane. Hence, actin polymerization takes place at the membrane and a branched actin network is formed through the Arp2/3-complex mechanism, building a branched actin cortex underneath the membrane (3). To prevent nucleation of filamentous actin from globular actin in the bulk, we use profilin (10) in a 3:1 proportion to actin monomers. Using 10% of fluorescent actin monomers, the actin cortex appears as a fluorescent shell inside the liposome within 5–20 min at 23°C, as shown in Fig. 1 B. We will refer to this system as "cortex" liposomes. In parallel, we use a cortex-free system, which we call "bulk" liposomes, where the liposome contains exclusively actin without the actin machinery that
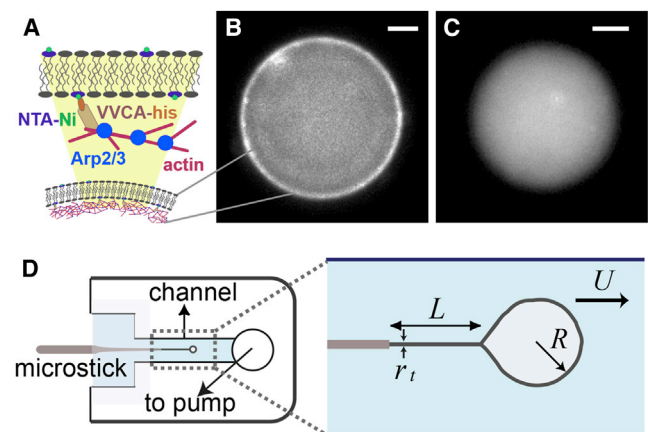
FIGURE 1 Experimental setup. (A) Schematic representation of protein assembly to form the biomimetic actin cortex. (B) Fluorescent image of an actin cortex, seen as a bright halo at the membrane of the liposome. (C) Liposome with actin in the bulk. Both scale bars are 5 μm. (D) Scheme of the experimental chamber and the principle of hydrodynamic tube-pulling technique. A constant flow U is applied inside the channel, applying a hydrodynamic force $F_h = 6\pi\eta UR$ on the liposome (Movie S1). The length L is measured as a function of time for a given F_h.

polymerizes actin into filaments. Indeed, in these conditions, actin does not polymerize at the membrane and remains in the bulk of the liposome, as seen in Fig. 1 C. This system is used as a reference to characterize the role of the biomimetic cortex on membrane mechanics.

For each trial, bulk and cortex liposomes are prepared separately with the exact same buffers except that the Arp2/3 complex, profilin, and VVCA-His are omitted from the bulk liposomes (see the Materials and Methods). Actin in both types of liposomes differs only by the fluorophore it carries. Liposomes are then introduced into the experimental chamber containing the external buffer. Tube-pulling measurements are performed on each type of liposome in random order. This approach allows us to have the two populations in the most comparable conditions.

Mechanical resistance of cortex liposomes revealed by tube-pulling assay

The mechanics of liposomes are characterized by pulling membrane tubes using a hydrodynamic flow. The scheme of the experiment is shown in Fig. 1 D: a liposome of radius R is attached to a microstick through biotin-streptavidin links and brought inside the microfluidic channel where a constant flow, U, is applied in the direction parallel to the stick, exerting a hydrodynamic force $F_h = 6\pi\eta RU$ on the liposome, where η is the viscosity of the medium. The liposome in the flow feels a pulling force $F_p = 6\pi\eta R(U - \dot{L})$, where $\dot{L}$ is the tube elongation rate. In fact, the static force needed to pull a tube is given by $F = 2\pi\sqrt{2\kappa\sigma}$, where σ is the membrane tension, and κ is the bending modulus of the membrane (11). The balance of forces during the pulling of the tube is thus given by

$$6\pi\eta R(U - \dot{L}) = 2\pi\sqrt{2\kappa\sigma}. \qquad (2)$$

In the presence of adhesion of the membrane to the underlying cytoskeleton, σ has to be replaced by $\sigma + W$, where W is the adhesion energy per unit area to detach the membrane from the cortex (12).

The tube dynamics are studied by analyzing tube length, $L(t)$, as a function of time by video tracking. Fig. 2 A shows typical tube extrusion curves from cortex (*red*) and bulk (*blue*) liposomes, where the applied flow is increased in steps every 60–90 s (Movie S1 in the Supporting Material). Each step has the same feature: a rapid elongation during the first few seconds followed by a slow linear increase, as seen in the inset of Fig. 2 A. The characteristic time needed to change the value of the flow is <1 s, small compared to the characteristic time τ of the rapid elongation phase (~10 s). We point out that the $L(t)$ curves corresponding to cortex liposomes are visibly below the ones corresponding to bulk liposomes. At a given force and a given time, much shorter tubes are pulled from a cortex liposome than a bulk liposome, and at larger times the rate of elongation
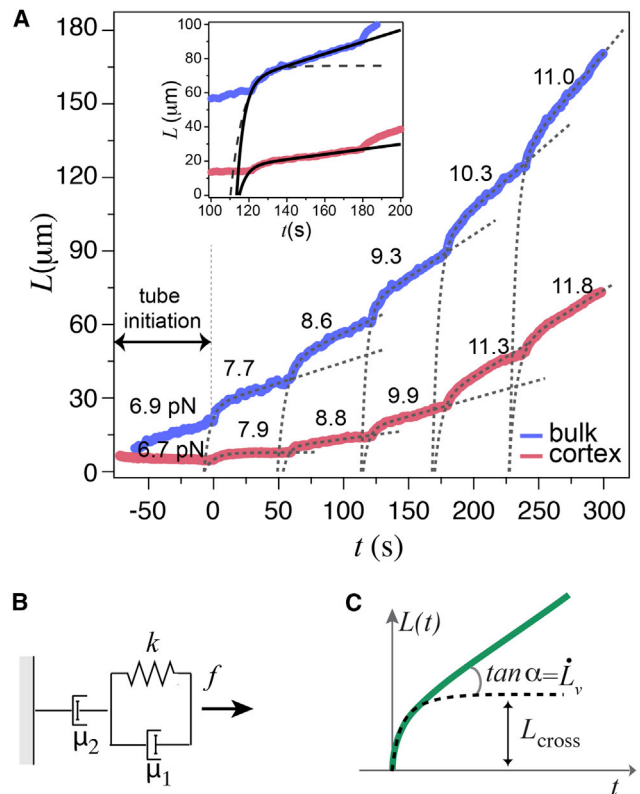
FIGURE 2 Tube dynamics of cortex and bulk liposomes. (*A*) Stepwise tube extrusion from liposomes with an actin cortex attached to the bilayer membrane (*red*) and with actin in bulk (*blue*). The numbers above each step indicate the hydrodynamic flow force, $F_h = 6\pi\eta UR$, in pN. At $F_h = 6.7$ pN (*red curve*), the tube initiated from the cortex liposome retracts itself, showing that $6.7 < F_0 < 7.9$ pN, whereas for bulk liposome (*blue curve*), $F_0 < 6.9$ pN. The solid curves in the inset and the dotted lines in the main figure are adjustments to the extrusion curves with a modified KV body schematized in (*B*). The dashed line in the inset of (*A*) shows the case where $\mu_2 = \infty$. The R^2 for the successive fits for the bulk liposomes are 0.97 for the first curve and 0.99 for the remaining, and for the cortex liposome, 0.97 for the first two, and 0.99 for the next three. (*B*) Modified KV body: a dashpot with a damping coefficient μ_2 is added in series to a KV body comprising a spring constant k and a dashpot with a damping coefficient μ_1 assembled in parallel and pulled by a force f. (*C*) $L(t)$ curve corresponding to the mechanical model represented in (*B*). At short times, the tube elongates rapidly to a length L_{cross}, after which the elongation occurs at a constant speed $\dot{L}_v$.

is reduced for cortex liposomes. We will analyze these two regimes by considering a mechanical model consisting of springs and dashpots.

DISCUSSION

Kelvin-Voigt mechanical analog

Such a behavior of steep increase followed by a slow linear increase has a mechanical analog of a modified Kelvin-Voigt (KV) body made of a spring and a dashpot in parallel, with a spring constant k and a damping coefficient μ_1, connected in series to a second dashpot with a damping

coefficient μ_2 as shown in Fig. 2 B. For a fixed force f, this model results in the following equation for the displacement $L(t)$, shown schematically in Fig. 2 C:

$$L(t) = L_{\text{cross}}\left(1 - e^{-t/\tau}\right) + \dot{L}_v t. \qquad (3)$$

Here, $\tau = \mu_1/k$ is the characteristic time of the elastic deformation, $L_{\text{cross}} = f/k$, and $\dot{L}_v = f/\mu_2$.

Mechanical parameters extracted from KV model

Equation 3 is valid for the first step when at $t = 0$, $L = 0$; however, for the consecutive steps, Equation 3 is modified as described in the Material and Methods. Therefore, we adjust Eq. 1 to deduce the following three mechanical parameters: the crossover length from the initial viscoelastic to viscous regime, L_{cross}; the characteristic time τ; and a long-term constant flow rate $\dot{L}_v$, which leads to μ_2.

The solid lines in the inset of Fig. 2 A show an example of the adjustments of the $L(t)$ curves with Eq. 1 for the two types of liposomes using the viscoelastic model in Fig. 2 B. An analysis of all the data is displayed in Fig. 3. We observe that 1) L_{cross} increases linearly with F_h and vanishes for a finite value F_0 (Fig. 3 A); and 2) the slope of $L_{\text{cross}}(F)$ is much larger for bulk than for cortex liposomes (Fig. 3 B). Indeed, with $f = F_h - F_0$, the elastic coefficient is found to be $k = (4 \pm 1) \times 10^{-8}$ N/m (mean $\pm$ SE) for bulk liposomes whereas it is ~10 times

higher, $k = (32 \pm 10) \times 10^{-8}$ N/m (mean $\pm$ SE), for cortex liposomes. This can also be seen from the histogram shown in Fig. 3 C, where k is obtained from each L_{cross} separately. We have also observed that the elastic coefficient k does not depend on the magnitude of the force increment (Fig. S1). The damping coefficient also shows a drastic difference between bulk, $\mu_2 = (1.4 \pm 0.1) \times 10^{-5}$ N.s/m (mean $\pm$ SE) and cortex, $\mu_2 = (15 \pm 3) \times 10^{-5}$ N.s/m (mean $\pm$ SE) liposomes. We have found little variation in the characteristic time, $\tau = 5.5 \pm 0.5$ s (mean $\pm$ SE) for bulk and $\tau = 4.5 \pm 0.3$ s (mean $\pm$ SE) for cortex liposomes, and that it does not vary with force (Figs. S2 and S3).

Tube extrusion critical force

If σ_0 is the initial membrane tension before the tube is pulled, the critical force to extrude a tube is $F_0 = 2\pi\sqrt{2\kappa\sigma_0}$ for bulk liposomes and $F_0 = 2\pi\sqrt{2\kappa(\sigma_0 + W)}$ for cortex liposomes (see remarks above). Experimentally, the measurement of F_0 is not straightforward because to initiate the first tube, for an adhesion patch on the microstick as small as 1 μm in radius, a force threshold of ~$50 \times F_0$ needs to be overcome (13). Therefore, to initiate a tube, we momentarily increase the force by moving the microstick, with the liposome attached to it, back and forth in parallel to the flow direction (Movie S2). To determine F_0, we first increase F_h by small increments of 0.5–1 pN and we repeat the back-and-forth movement of the microstick until we succeed in pulling a
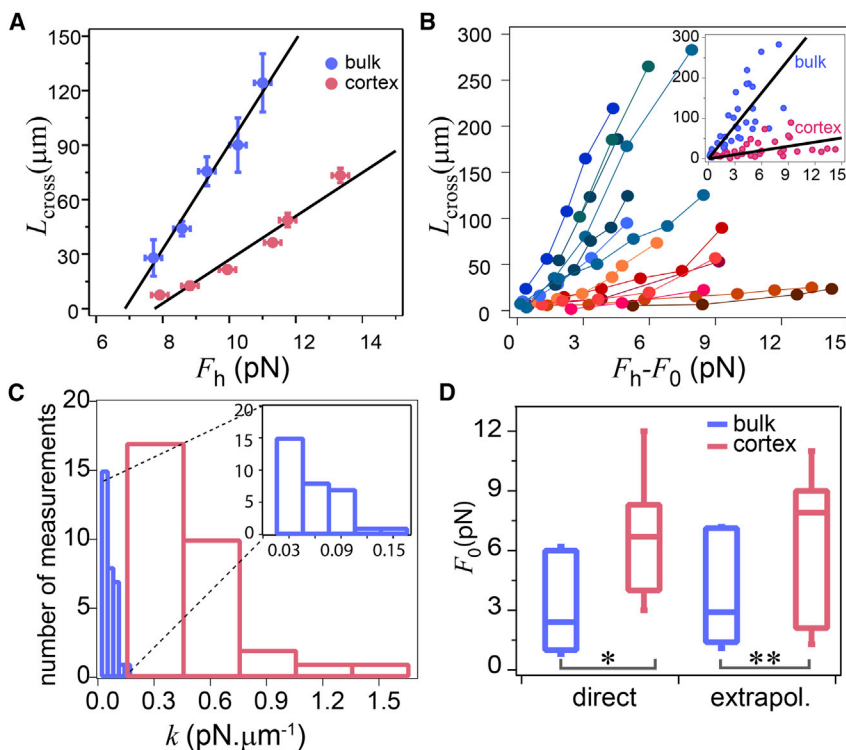

FIGURE 3 Short-term viscoelastic deformation of the membrane tube as a function of pulling force. (A) Crossover length L_{cross} for bulk and cortex liposomes as the pulling force is increased in steps. Blue and red curves correspond to bulk and cortex liposomes, respectively. The radius of the bulk and the cortex liposomes is $R_0 = 10 \pm 0.5$ μm. (B) L_{cross} for several liposomes as a function of $F_h - F_0$, where F_0 is the tube initiation force. (Inset) All data together. Linear regression demonstrates a mean slope for bulk and cortex liposomes proportional to the inverse of an effective bending modulus k (see text). (C) Histogram of $k = f/L_{\text{cross}}$ for all data points, giving $k = (4.4 \pm 0.4) \times 10^{-8}$ N/m (mean $\pm$ SE) for bulk and $k = (38 \pm 6) \times 10^{-8}$ N/m (mean $\pm$ SE) for cortex liposomes; $p < 10^{-14}$. (D) Critical extrusion force F_0 for bulk and cortex liposomes obtained by both direct (*$p < 0.1$) and extrapolation approaches (**$p < 0.5$).

tube. Once a tube is formed, we slightly vary the force until we get a stable short tube at a minimum force. This value corresponds to our direct estimate of F_0. We find an average value of $F_0 = 3 \pm 1$ pN (mean $\pm$ SE) for bulk and $F_0 = 6 \pm 1$ pN (mean $\pm$ SE) for cortex liposomes. A second way of estimating F_0 is by obtaining the intercept of L_{cross} versus F_h. As we show in Fig. 3 A, the intercept corresponds to F_0 for two liposomes, showing that F_0 for cortex liposomes is larger than for bulk liposomes. Note that F_0 may vary depending on the history of the tube. However, we do not have access to this variation in our experiments. Therefore, we consider F_0 to be constant for the consecutive steps.

On average, we find $F_0 = 4 \pm 1$ pN (mean $\pm$ SE) for bulk and $F_0 = 7 \pm 1$ pN (mean $\pm$ SE) for cortex liposomes, which is consistent with the estimated values for F_0 from the tube initiation approach (Fig. 3 D).

The value of the adhesion energy W between the membrane and the cortex can be derived from the ratio of $F_0^{cortex}/F_0^{bulk} = \sqrt{1 + W/\sigma_0}$, which is ~2 (Fig. 3 D). Therefore, in our experiments, $W \approx 3 \times \sigma_0$. Hence, both adhesion and membrane tension need to be taken into account for cortex liposomes. Note that for cells in nonadhering conditions, W is orders-of-magnitude larger than σ_0, thus the increase of σ_0 is masked by W entirely and the tube-pulling force is governed by cortex-membrane adhesion (14,15). In adhering motile cells such as in keratocytes, σ_0 and W are comparable (16), and both contribute to the pulling force.

Model of viscoelastic tube extrusion

When a liposome is submitted to a flow above a threshold force F_0, and for times smaller than τ, the regime is elastic and tube length tends toward L_{cross}. However, for longer times, $t > \tau$, a slow increase in $L(t)$ corresponds to a viscous regime. We discuss here these two regimes of hydrodynamic tube extrusion for bulk and cortex liposomes.

Elastic regime

Let us first remind the reader of the elastic regime for bare liposomes as previously studied in the case of DOPC liposomes (7), taking into account the increase in membrane tension σ when a pulled tube unwinds membrane fluctuations. As shown by Helfrich and Servuss (17), when the area of a liposome is altered by an amount ΔA, its surface tension varies from σ_0 to σ according to the following relationship:

$$\frac{\Delta A}{A_p} = \frac{k_B T}{8\pi\kappa} \ln\frac{\sigma}{\sigma_0} + \frac{\sigma - \sigma_0}{K_s}. \tag{4}$$

Here $A_p = A\pi R_0^2$ is the membrane projected area of the liposome with a radius R_0; $k_B T$ is the thermal energy; κ is the bending modulus of the membrane already defined above; and K_s is the stretching coefficient. The first term

on the right is the entropic term describing the increase of the membrane tension corresponding to smoothing of thermal membrane undulations, whereas the second term refers to the increase in the distance between lipid molecules resulting in membrane stretching in high tension regimes ($\sigma > 10^{-3}$ N/m) (18).

Considering that the maximum pulling forces used in our experiments are ~10 pN, the maximum tension can be estimated by taking $\kappa = 5 k_B T$ from $\sigma = F^2/8\pi^2\kappa = 6 \times 10^{-5}$ N/m, showing that the contribution of the second term is small, and hence negligible; this is also confirmed by taking $K_s = 0.1$ N/m (7,19), and the range of membrane tensions involved in our experiments. Therefore, we can simplify Eq. 4 to

$$\frac{\Delta A}{A_p} = \frac{k_B T}{8\pi\kappa} \ln\frac{\sigma}{\sigma_0}. \tag{5}$$

When a tube of length $L(t)$ is pulled, the change in the area of the liposome is $\Delta A = 2\pi r_t L(t)$, where $r_t = \sqrt{\kappa/2\sigma} = 2\pi\kappa/F_p$ is the tube radius (11). Rewriting Eq. 5 in terms of $L(t)$ and F_p ($F_p = 6\pi\eta R(U - \dot{L})$), we obtain

$$L(t) = \frac{k_B T R_0^2}{4\pi^2\kappa^2} F_p \ln\frac{F_p}{F_0}. \tag{6}$$

L_{cross} is derived from Eq. 6 for $F_p = F_h$, which corresponds to $\dot{L}_v = 0$,

$$L_{cross} = \frac{1}{k} F_h \ln\frac{F_h}{F_0}, \tag{7}$$

where $k = 4\pi^2\kappa^2/k_B T R_0^2$ is the elastic modulus. For F_h close to F_0, we obtain a linear relationship between F_h and L_{cross} as

$$L_{cross} = \frac{1}{k}(F_h - F_0). \tag{8}$$

Integration of Eq. 6 leads to the general expression of $L(t)$ in the elastic regime,

$$L(t) = L_{cross}(1 - e^{-t/\tau}), \tag{9}$$

where $\tau = 3\eta R_0^3 k_B T/2\pi\kappa^2$. Note that Eq. 9 corresponds exactly to the first term of Eq. 3.

Data in Fig. 3, A and B, are approximated by a linear relationship (solid lines) using Eq. 8. The inverse of the slope gives k and the intercept gives an estimate for F_0. Such an analysis is correct for bulk liposomes (blue curve). However, the same linear behavior is also found for cortex liposomes (red curves, Fig. 3, A and B).

We first analyze k values for bulk liposomes. The distribution of $k = (F_h - F_0)/L_{cross}$ is shown on the histogram of Fig. 3 C. From the slopes of the adjustments to Fig. 3 B, we obtain an average value of $k = 4 \pm 1 \times 10^{-8}$ N/m for

liposome radii ranging between 8.7 and 11.5 μm, which corresponds to $\kappa = 5 \pm 1\ k_BT$. The average critical pulling force is $F_0 = 4 \pm 1$ pN, as shown on Fig. 3 D. Using $\sigma_0 = F_0^2/(8\pi^2\kappa)$, we obtain the resting surface tension of the liposomes $\sigma_0 = 9 \pm 1 \times 10^{-6}$ N/m. The values for κ and σ_0 are comparable to values reported previously for bare liposomes (7), implying that the mechanical properties of the membrane are not significantly affected by the presence of an encapsulated actin monomer solution. The characteristic time τ of Eq. 9 can be estimated by taking $\eta = 10^{-3}$ Pa.s, and $\kappa = 5\ k_BT$, which gives $\tau = 5 \pm 2$ s. This value compares well with the values obtained experimentally, justifying the use of the mechanical model introduced in the previous section.

For cortex liposomes, where the membrane is attached to the actin cortex with an adhesion energy W, the force modifies to $F_p = 2\pi\sqrt{2\kappa(\sigma + W)}$ (12). Taking this into account, Eq. 5 becomes

$$L(t) = \frac{k_BTR_0^2}{8\pi^2\kappa^2}F_p \ln\frac{F_p^2 - 8\pi^2\kappa W}{F_0^2 - 8\pi^2\kappa W}. \tag{10}$$

As for obtaining Eq. 8 from Eq. 6, L_{cross} is then derived for $F_p = F_h$, which corresponds to $\dot{L}_v = 0$; for F_h close to F_0, L_{cross} reads

$$L_{\text{cross}} = \frac{1}{k_W}(F_h - F_0), \tag{11}$$

with $k_W = 4\pi^2\kappa^2/k_BTR_0^2(1 - (W/W + \sigma_0))$. Equation 11 shows that for cortex liposomes, k_W should be smaller than the k for bulk liposomes. However, if we compare the values of L_{cross} versus F_h–F_0, we see a clear separation between the bulk (blue) and cortex (red) liposomes. For cortex liposomes, we find $k_W = 32 \pm 10 \times 10^{-8}$ N/m, a much higher value than for bulk liposomes, where $k = 4 \pm 1 \times 10^{-8}$ N/m, as can be seen on the histogram of Fig. 3 C. We note that k depends on two parameters: the membrane bending modulus κ, and the total available area, $A_p = 4\pi R_0^2$, for pulling a tube (see derivation of Eqs. 4 and 5). Because κ is the same for both types of liposomes (same lipid composition and no nonspecific interaction between filamentous actin and the membrane (2,3)), the increase of the elastic coefficient suggests that the available surface for pulling a tube is no longer A_p but is reduced to $\alpha \times 4\pi R_0^2$, where $\alpha < 1$. We can consider that the attachment of an actin cortex to the membrane creates patches that limit the available surface to pull a tube. This corral model was introduced to explain the confined motion of proteins in cell membranes (20) and applied to liposomes filled with polymer gels adhered to the lipid bilayer (21). A recent study (22) has put in evidence the influence of the plasma membrane compartmentalization by the cortical actin cytoskeleton on the diffusion of lipid molecules in the cell membrane. For cortex liposomes, the expression of k_W reads

$$k_W = \frac{k}{\alpha}\left(1 - \frac{W}{W + \sigma_0}\right). \tag{12}$$

As estimated above, $W \approx 3\sigma_0$, therefore, $\alpha \approx 3\%$. The characteristic size of the patch is then given by $\sqrt{\alpha}R_0$ with $\alpha = 3\%$ and $R_0 \approx 10\ \mu$m, and the corral size is of micron order, in agreement with Qian et al. (23). Note that the bending modulus of the cortex is higher than that of the membrane in our system, as in cells (24). Therefore, we consider here that the deformability of the cortex is negligible.

Viscous regime

At longer times $t > \tau$, corresponding to $L > L_{\text{cross}}$, the tube elongates with a constant velocity $\dot{L}_v$, as shown on Fig. 2 A. Fig. 4 shows our measured values for $\dot{L}_v$ as a function of the applied force F_h for both types of liposomes.

Note that a long-term relaxation has been observed in a similar system from the dynamic-force relaxation experiments (6). The viscous regime corresponding to this condition was related to a putative diffusion process arising from the dynamic reorganization of the lipid molecules inside the membrane. Here, the long-term relaxation is observed at a constant pulling force. We address thoroughly which mechanism can give rise to a linear increase of tube length with time, observed in our experiments.
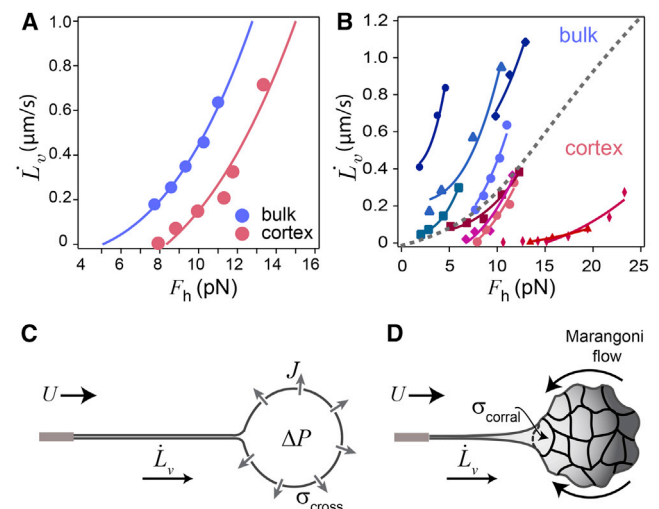

FIGURE 4 Viscous response for bulk and cortex liposomes. (A) $\dot{L}_v$ versus F_h for bulk (blue) and cortex (red) liposomes for liposomes represented in Fig. 2 A adjusted with a cubic function. The adjustment parameter gives the permeability, P_w, of the membrane for bulk liposomes and membrane viscosity for cortex liposomes. (B) $\dot{L}_v$ as a function of F_h for all liposomes (dashed line separates the two groups). (C) Sketch of a bulk liposome in the leakout regime; the tube elongates at a constant speed $\dot{L}_v$ when the membrane tension reaches a constant value σ_{cross}. (D) Sketch of a cortex liposome in the Marangoni regime. (Arrows) Marangoni flow from the floppy region toward the tense region at the tube neck.

First we will consider the case of bulk liposomes. The elongation at constant velocity of the tube length is reminiscent of tube dynamics when pores are incorporated into the membrane of liposomes (25,26). As a tube is pulled, the surface tension of the membrane increases. The Laplace pressure $2\sigma/R$ induces a slow leakout of the internal liquid. The radius of the liposome decreases, and the excess area increases. A stationary regime is reached, when the gain of the area due to liposome deswelling is transferred into the tube. Equation 2 shows that if $\dot{L}_v$ becomes constant, σ reaches a constant value σ_{cross}; this corresponds to the crossover between elastic and viscous regimes, corresponding to $L \sim L_{\text{cross}}$.

The extrusion of tubes from porous liposomes decorated with n proteic pores of size a has been studied previously in Borghi et al. (25). The Poiseuille's law for one pore can be written in a scaling approach as $\eta V/a^2 \approx \sigma/aR$, where V is the water velocity through the pore. The flux per pore is $J_p = Va^2 \sim \sigma a^3/\eta R$. The total flux is therefore $J = nJ_p$. Introducing Σ, the density of pores, and A, the area of the liposome, we get $n = \Sigma A$ and the total flux J including the exact numerical coefficient (27), which is

$$J = \Sigma \frac{A}{3\eta} \frac{2\sigma}{R} a^3. \tag{13}$$

Equation 13 has been extended for the permeation of the water molecule through the lipid bilayer where a^3 is the molecular volume of water $v_0 \approx 3 \times 10^{-29}$ m^3. Therefore, J can be rewritten as

$$J = AP_w \frac{v_0}{k_B T} \frac{2\sigma}{R}, \tag{14}$$

where $P_w = \Sigma k_B T/3\eta$. Equation 14 holds for the intrinsic porosity of lipid bilayers, measured previously to be ~$P_w = 100$ μm/s for a polyunsaturated phosphatidylcholine lipid membrane (28). However, as the tension of the membrane increases, transient pores open and close (29), leading to an increase of P_w. The leakout of the internal liquid leads to a deswelling of the liposome,

$$4\pi R^2 \dot{R} = -AP_w \frac{v_0}{k_B T} \frac{2\sigma}{R}; \tag{15}$$

then,

$$\dot{R} = -P_w \frac{v_0}{k_B T} \frac{2\sigma}{R}. \tag{16}$$

Combining Eqs. 2 and 16, and considering that the area decrease of the liposome is related to the increase of tube length through $-8\pi R\dot{R} = 2\pi r_t \dot{L}_v$, we derive the following relationship between the tube elongation rate $\dot{L}_v$ and the hydrodynamic flow rate U as $(U - \dot{L}_v)^3 = U_{p0}^2 \dot{L}_v$, (17), where

$$U_{p0} \simeq \frac{\kappa}{(3\eta R_0)^{3/2}} \left(\frac{k_B T}{4P_w v_0} \right)^{1/2}. \tag{18}$$

We estimate U_{p0} as the following, taking $P_w = 100$ μm/s for polyunsaturated phosphatidylcholine lipid membrane (28), with $R_0 = 10$ μm and $\kappa = 5$ $k_B T$, $U_{P0} \approx 2$ cm/s. This value is much larger than U, which is in the range of 10–100 μm/s. Hence for $U_{p0} >> U$, Eq. 17 becomes

$$\dot{L}_v \approx \frac{U^3}{U_{P0}^2} \approx C_l F^3, \tag{19}$$

where $C_l = (4v_0 P_w)/[(2\pi)^3 \kappa^2 k_B T]$. The solid lines in Fig. 4, A and B, show the adjustments to the data with Eq. 19 for bulk liposomes, giving $C_l = 1.1 \pm 0.6 \times 10^{27}$ N^{-3}.s.m^{-1}. We obtain $P_w = 4300 \pm 2300$ μm/s. This large value of permeability compared to the values reported for liposomes at rest (28) confirms that at high membrane tension, the membrane becomes more permeable.

Let us now address the viscous regime observed for cortex liposomes. Due to the corral effect, the dissipation mechanism is different than in bulk liposomes. For cortex liposomes, the lipid mobility is strongly reduced and the membrane tension does not equilibrate rapidly because the tube is pulled from a small patch or corral domain. In this case, $\dot{L}_v$ is controlled by a Marangoni flow from the low tension region of the corral domain toward the tense region at the tube neck. The dynamics of membrane tube extrusion as a function of binder density, ν, has been studied before in the case of red blood cells (14). The relationship between F_h and $\dot{L}_v$ is given by

$$F_h^3 - F_0^2 F_h = (2\pi)^3 2\kappa^2 \nu \eta_e \dot{L}_v \log R/r_t, \tag{20}$$

where η_e is the membrane surface viscosity. Previous measures of η_e for cells show a variation between 10^{-4} and 10^{-9} Pa.s.m (14,30–33). Adjusting the curves for cortex liposomes shown in Fig. 4 by $\dot{L}_v = C_m(F_h^3 - F_0^2 F_h)$, where $C_m = [(2\pi)^3 2\kappa^2 \nu \eta_e \log R/r_t]^{-1}$, we obtain $C_m = 1.3 \pm 0.5 \times 10^{26}$ N^{-3}.s.m^{-1}, giving $\nu \eta_e = 1.9 \pm 0.9 \times 10^{10}$ Pa.s/m. To evaluate η_e, we first estimate the binder density ν, which is related to the distance between binding sites ξ by $\nu \sim 1/\xi^2$. If we consider that all Arp2/3-complex molecules saturate the VVCA sites, for a liposome of radius 10 μm, and Arp2/3 concentration of 0.45 μM, we find $\xi \approx 30$ nm, giving $\nu \approx 10^{15}$ m^{-2} and $\eta_e \approx 10^{-5}$ Pa.s.m, consistent with the membrane viscosity estimated for cells. Therefore, our experiments using stripped-down systems of cell-size liposomes mimicking cells are able to reproduce a cell behavior.

To summarize, the viscous regime of bulk and cortex liposome tube pulling can be explained by two different mechanisms. In the case of bulk liposomes, the viscous regime is explained by a leakout of the internal liquid through the

permeable membrane. On the other hand, for cortex liposomes, the tension increases locally, due to the corral domains giving rise to a flow of lipids (Marangoni effect) from the floppy part toward the tube (see in Fig. 4, C and D). A surprising feature is that both phenomena give the same scaling law: $\dot{L}_v \sim F_h^3$ (Eqs. 19 and 20), but numerical coefficients differ by a factor of 10: $C_l = 1.1 \pm 0.6 \times 10^{27} \, N^{-3}.\mathrm{s.m}^{-1}$ and $C_m = 1.3 \pm 0.5 \times 10^{26} \, N^{-3}.\mathrm{s.m}^{-1}$ ($p < 10^{-7}$), therefore explaining a slower velocity of extrusion in the presence of an actin cortex.

CONCLUSIONS

In this article, we study the mechanics of liposomes when an artificial actin cortex is reconstructed on the inner layer liposome. Using a lipid tube extrusion technique based on hydrodynamic flow, we show that the tube dynamics for liposomes with a cortex is significantly different compared to liposomes containing a nonpolymerizing actin solution. According to our data at comparable forces, cortex liposomes deform much less and the tube extrusion velocity is much smaller. We propose that polymerization of actin on the inner leaflet of the liposome creates patches that limit the size of the available area for pulling a tube. These patches are associated to a reduced lipid mobility that explains differences in the dynamics of the tube extrusion. Recently, a similar effect of cortical actin on lipid diffusion has been put in evidence in fibroblast cells (22). The presence of actin at the membrane drastically changes the classical laws of membrane elasticity and viscous dissipation.

SUPPORTING MATERIAL

Three figures and two movies are available at http://www.biophysj.org/biophysj/supplemental/S0006-3495(15)01159-5.

AUTHOR CONTRIBUTIONS

K.G., F. B.-W., and C.S. designed research; K.G. performed research; J.M. designed, purified, and characterized proteins; L.-L.P. prepared the liposome fabrication method; K.G., F. B.-W., and C.S. analyzed data; and K.G., F.B.-W., and C.S. wrote the article.

ACKNOWLEDGMENTS

REFERENCES

1. Charras, G. T., C. K. Hu, …, T. J. Mitchison. 2006. Reassembly of contractile actin cortex in cell blebs. *J. Cell Biol.* 175:477–490.

2. Limozin, L., M. Bärmann, and E. Sackmann. 2003. On the organization of self-assembled actin networks in giant vesicles. *Eur. Phys. J. E Soft Matter.* 10:319–330.

3. Pontani, L. L., J. van der Gucht, …, C. Sykes. 2009. Reconstitution of an actin cortex inside a liposome. *Biophys. J.* 96:192–198.

4. Murrell, M., L. L. Pontani, …, C. Sykes. 2011. Spreading dynamics of biomimetic actin cortices. *Biophys. J.* 100:1400–1409.

5. Schäfer, E., T. T. Kliesch, and A. Janshoff. 2013. Mechanical properties of giant liposomes compressed between two parallel plates: impact of artificial actin shells. *Langmuir.* 29:10463–10474.

6. Campillo, C., P. Sens, …, C. Sykes. 2013. Unexpected membrane dynamics unveiled by membrane nanotube extrusion. *Biophys. J.* 104:1248–1256.

7. Borghi, N., O. Rossier, and F. Brochard-Wyart. 2003. Hydrodynamic extrusion of tubes from giant vesicles. *Europhys. Lett.* 75:666–672.

8. Carvalho, K., J. Lemière, …, C. Sykes. 2013. Actin polymerization or myosin contraction: two ways to build up cortical tension for symmetry breaking. *Phil. Trans. R. Soc. B.* 368:20130005.

9. Pautot, S., B. Frisken, and D. Weitz. 2003. Production of unilamellar vesicles using an inverted emulsion. *Langmuir.* 19:2870–2879.

10. Blanchoin, L., and T. D. Pollard. 1998. Interaction of actin monomers with *Acanthamoeba* actophorin (ADF/cofilin) and profilin. *J. Biol. Chem.* 273:25106–25111.

11. Derényi, I., F. Jülicher, and J. Prost. 2002. Formation and interaction of membrane tubes. *Phys. Rev. Lett.* 88:238101.

12. Waugh, R. E., and R. G. Bauserman. 1995. Physical measurements of bilayer-skeletal separation forces. *Ann. Biomed. Eng.* 23:308–321.

13. Koster, G., A. Cacciuto, …, M. Dogterom. 2005. Force barriers for membrane tube formation. *Phys. Rev. Lett.* 94:068101.

14. Brochard-Wyart, F., N. Borghi, …, P. Nassoy. 2006. Hydrodynamic narrowing of tubes extruded from cells. *Proc. Natl. Acad. Sci. USA.* 103:7660–7663.

15. Dai, J., and M. P. Sheetz. 1999. Membrane tether formation from blebbing cells. *Biophys. J.* 77:3363–3370.

16. Lieber, A. D., S. Yehudai-Resheff, …, K. Keren. 2013. Membrane tension in rapidly moving cells is determined by cytoskeletal forces. *Curr. Biol.* 23:1409–1417.

17. Helfrich, W., and R. Servuss. 1984. Undulations, steric interaction and cohesion of fluid membranes. *Il Nuovo Cimento D.* 3:137–151.

18. Evans, E., and W. Rawicz. 1990. Entropy-driven tension and bending elasticity in condensed-fluid membranes. *Phys. Rev. Lett.* 64:2094–2097.

19. Upadhyaya, A., J. R. Chabot, …, A. van Oudenaarden. 2003. Probing polymerization forces by using actin-propelled lipid vesicles. *Proc. Natl. Acad. Sci. USA.* 100:4521–4526.

20. Saxton, M. J. 1995. Single-particle tracking: effects of corrals. *Biophys. J.* 69:389–398.

21. Kremer, S., C. Campillo, …, A. Viallat. 2008. Nanotubes from gelly vesicles. *Europhys. Lett.* 75:666–672.

22. Andrade, D. M., M. P. Clausen, …, C. Eggeling. 2015. Cortical actin networks induce spatio-temporal confinement of phospholipids in the plasma membrane—a minimally invasive investigation by STED-FCS. *Sci. Rep.* 5:11454.

23. Qian, H., M. P. Sheetz, and E. L. Elson. 1991. Single particle tracking. Analysis of diffusion and flow in two-dimensional systems. *Biophys. J.* 60:910–921.

24. Tabdanov, E., N. Borghi, …, J.-P. Thiery. 2009. Role of E-cadherin in membrane-cortex interaction probed by nanotube extrusion. *Biophys. J.* 96:2457–2465.

25. Borghi, N., S. Kremer, …, F. Brochard-Wyart. 2006. Tube extrusion from permeabilized giant vesicles. *Europhy. Lett.* 75:666.

26. Lemiere, J., K. Guevorkian, …, T. Betz. 2013. α-Hemolysin membrane pore density measured on liposomes. *Soft Matter.* 9:3181–3187.

27. Guyon, E., J. Hulin, …, C. Mitescu. 2001. Physical Hydrodynamics. Oxford University Press, Oxford, UK.

28. Olbrich, K., W. Rawicz, …, E. Evans. 2000. Water permeability and mechanical strength of polyunsaturated lipid bilayers. *Biophys. J.* 79:321–327.

29. Brochard-Wyart, F., P. deGennes, and O. Sandre. 2000. Transient pores in stretched vesicles: role of leak-out. *Phys. A Stat. Mech. Appl.* 278:32–51.

30. Waugh, R. E. 1982. Surface viscosity measurements from large bilayer vesicle tether formation. II. Experiments. *Biophys. J.* 38:29–37.

31. Evans, E. A., and R. M. Hochmuth. 1976. Membrane viscoelasticity. *Biophys. J.* 16:1–11.

32. Golan, D. E., and W. Veatch. 1980. Lateral mobility of band 3 in the human erythrocyte membrane studied by fluorescence photobleaching recovery: evidence for control by cytoskeletal interactions. *Proc. Natl. Acad. Sci. USA.* 77:2537–2541.

33. Roth, K. B., C. D. Eggleton, …, D. W. Marr. 2013. Measuring cell mechanics by optical alignment compression cytometry. *Lab Chip.* 13:1571–1577.